IEEE Access
Multidisciplinary | Rapid Review | Open Access Journal

Received December 13, 2019, accepted December 23, 2019, date of publication December 26, 2019,
date of current version January 7, 2020.

Digital Object Identifier 10.1109/ACCESS.2019.2962556

Adaptive Optics Image Restoration via Regularization Priors With Gaussian Statistics

DONGMING LI[1,2], GUANGJIE QIU[1], AND LIJUAN ZHANG[3]
[1]School of Information Technology, Jilin Agricultural University, Changchun 130118, China
[2]College of Opto-Electronic Engineering, Changchun University of Science and Technology, Changchun 130022, China
[3]College of Computer Science and Engineering, Changchun University of Technology, Changchun 130012, China

Corresponding author: Lijuan Zhang (zhanglijuan@ccut.edu.cn)

This work was supported in part by the National Science Foundation of China under Grant 61806024, in part by the Science and Technology Plan Project of Changchun in Double Ten Project under Grant 18SS018, in part by the Scientific and Technological Research Project of the Department of Education in Jilin Province under Grant JJKH20180637KJ, and in part by the Department of Science and Technology of Jilin Province under Grant 20190301024NY.

ABSTRACT In order to compensate for any failure on the use of point spread function (blur kernel) estimation and image estimation priors, we propose a novel regularization priors scheme with adapting the parameter for image restoration involving adaptive optics (AO) images. Our scheme uses a maximum a posteriori estimation with Gaussian statistics on the image and point spread function (blur kernel). An efficient regularization prior method associated with alternating minimization method is described to obtain the optimal solution recursively. Our method is applied to synthetic and real adaptive optics images. After applying our restoration method, satisfying results are obtained. Experimental results demonstrate that our proposed model and method performs better for restoring images in terms of both subjective results and objective assessments than the current state-of-the-art restoring methods. In addition, our proposed method can be a new way to promote their performances for AO image restoration.

INDEX TERMS Image restoration, regularization priors, adaptive optics, Huber-Markov random field, maximum a posteriori.

I. INTRODUCTION

Seeing is the primary obstacle to obtaining high resolution astronomy observations from the ground. Atmospheric turbulence along the line of sight randomly distorts the wavefronts [1]. The result is geometrical distortions and blurring in the collected images. Adaptive optics (AO) is an important tool that allows solar astronomers to achieve diffraction limited observations from existing ground based telescopes [2], [3]. Adaptive optics facilitates solar imaging with expressively reduced low-order aberrations. However, due to the time scale of seeing evolution, AO only copes with limited high-order corrections.

Post-facto image restoration techniques can correct higher order aberrations, which is required for reaching the diffraction limit. Affected by many factors such as ambient light, attenuation, and scintillation, the image deconvolution problem seemed too difficult to solve for general blur kernels called the point spread functions (PSF). On the basis of the degraded image, the PSF and object image are jointly estimated, which is called the blind deconvolution method [10]. Deconvolution appears in a wide range of application areas, such as astronomical imaging, microscopy, medical imaging, remote sensing, photography, super-resolution applications, and motion tracking applications [11], [12].

The blind deconvolution problem is very challenging since it is hard to infer the original image and the unknown degradation only from the observed image [12]. In the past few decades, many image restoration techniques have been proposed to solve this problem under all kinds of conditions. Both single and multiframe restoration schemes are reported in the literature. A single-channel blind deconvolution method [16] is proposed by Ayers *et al.*, which is more complicated than the classical deconvolution problem. In order to handle the ill-posed nature of blind deconvolution to a great extent of considering multiple images, Tian *et al.*

The associate editor coordinating the review of this manuscript and approving it for publication was Jeon Gwanggil.

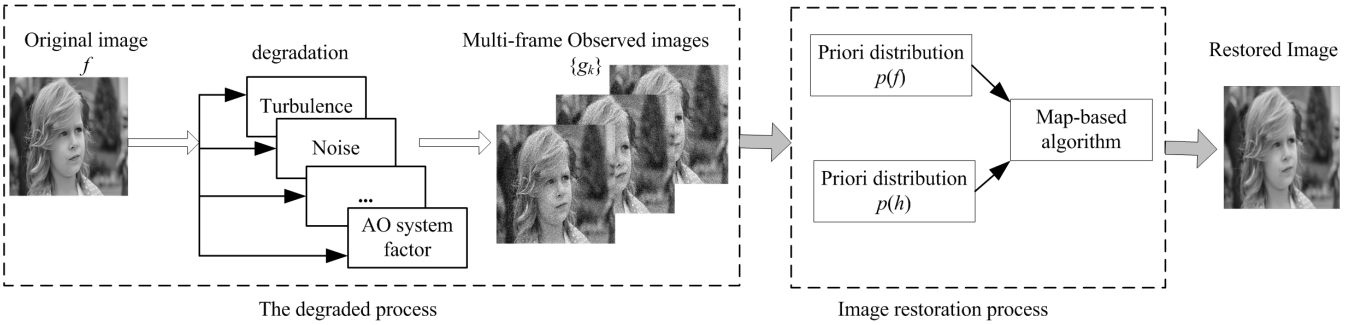

FIGURE 1. The flow chart of our proposed method for AO image restoration.

presented another multiframe restoration algorithm based on the frame selection techiques [17]. Approaches based on improved expectation maximization for AO image restoration was proposed in [18]. An adaptive image restoration method based on hierarchical neural network is proposed by Yap *et al.* [19]. They usually involved some regularizations which assured various statistical properties of the image or constrained the estimated image and/or restoration filter according to some assumptions [13]. Sroubek *et al.* developed a robust multichannel blind deconvolution algorithm based on an optimization problem with image and blur regularization terms [11]. Levin *et al.* in [14] claimed that the joint posterior probability of the image-blur pair favoring a trivial solution of the blur being a delta function was more appropriate. Other authors [4], [15] used the alternating maximum a posteriori (MAP) methods. However, they used ad hoc steps that often lacked rigorous explanation.

Here, we propose an adaptive optics image restoration method that can handle the point spread function and objective image estimation with better accuracy and speed. The method is based on MAP estimation, and it is formulated as a constrained optimization problem by using a regularization method. For the image regularization, we adopt the Huber-Markov random field (HMRF) method [6], and for the blur regularization, we use the constraint method proposed in [11]. Furthermore, our method solves the optimization problem in an iterative way by alternating between minimizations with respect to an image regularization term (f-step) and with respect to a blur kernel regularization term (h-step).

This paper is organized as follows. In Section II, we gives the statement of the AO image model. Then, the AO image restoration problem will be placed into a statistical model, using a MAP estimation. Section III builds the prior distributions of the original image and the blur kernel, and then the alternating minimization (AM) algorithm is built. Section IV presents experimental results for the AO image restoration techniques, quantitatively comparing the proposed method to other forms of image restoration methods on synthetic and real adaptive optics images. In Section V, the paper is concluded. The flow chart of this work is shown in Fig. 1.

II. MULTIFRAME AO IMAGE RESTORATION BASICS

A. ADAPTIVE OPTICS DEGRADED IMAGE MODEL

Single frame blind deconvolution amounts to estimating an image f from an observed image g, which can be expressed as

$$g(x) = f(x) \otimes h(x) + n(x), \quad x \in \Omega \tag{1}$$

where $h(x)$ is called the PSF (or blur kernel) and is unknown, $f(x)$ is the original image, $g(x)$ is the observed image, $n(x)$ is random additive noise, Ω is the support area of an image, x refers to a lexicographically ordered vector of the pixel coordinates in a 2-D image, that is $x = (x, y) \in \Omega$ (x is a position at the xth column and the yth row in the image), and the operator $\otimes$ denotes a 2-D convolution. The images are of size $N_1 \times N_2$.

Consider multiframe degraded AO images model that consists of M measurements of an original image f. The relationship between the observed sequence image g_m and the original image f is defined by

$$g_m(x) = f(x) \otimes h_m(x) + n_m(x), \quad 1 < m \leq M \tag{2}$$

where $h_m(x)$ is the point spread function of the m^{th} channel blur, $n_m(x)$ is the signal independent noise. Note that g_m is the only known variables. When no ambiguity arises, we drop index x from the notation. In the vector-matrix notation, Eq. (2) becomes

$$g_m = H_m f + n_m = F h_m + n_m \tag{3}$$

where matrices H_m and F perform convolution with h_m and f, respectively.

Our objective is to estimate $f(x)$ and $h(x)$ based on the degraded image $g(x)$ and prior information about the true image scene. This process is known as blind image deconvolution. Over the last few years, single frame blind deconvolution based on the Bayesian paradigm experiences a renaissance [5]. According the feature of the degraded AO images which is dominated by a strong homogeneous background, we assume that the AO image is further degraded with additive white Gaussian noise n with zero mean and variance σ^2.

B. STATISTICAL MODEL

Based on the Bayesian rule, simultaneous restoration of f and h amount to solving the standard maximum a posteriori estimation, which is

$$P(f, h|g) \propto P(g|f, h)P(f, h) = \frac{P(g|f, h)P(f)P(h)}{P(g)} \quad (4)$$

where P denotes probability, $P(g|f, h)$ is the noise distribution, $P(g)$, $P(f)$ and $P(h)$ are the prior distributions on the observed image, original image and PSF, respectively. $P(g)$ is a constant and can be omitted.

The MAP technique is to maximize the conditional probability for the PSF and the object image given a certain AO degraded image. That is

$$\left\{\hat{f}, \hat{h}\right\} = \arg\max_{\{f,h\}} \log P(f, h|g) \quad (5)$$

where $\log P(f, h|g)$ is the log-likelihood function. Maximization of the posterior $P(f, h|g)$ is equivalent to minimization of its negative logarithm, and according to Eq. (4), we have

$$\left\{\hat{f}, \hat{h}\right\} = \arg\min_{\{f,h\}} \{-\log P(g|f, h) - \log P(f) - \log P(h)\} \quad (6)$$

In order to compute the MAP estimation, the noise distribution $P(g|f, h) = P(n)|_{n=g-Hf}$ and the prior distribution $P(f)$ and $P(h)$ should be defined. For the noisy system model in Eq. (1), the conditional density has the Gaussian form [6]

$$P(g|f, h) = \frac{1}{(2\pi\sigma^2)^{\frac{N_1N_2}{2}}} \exp\left(\frac{-\|g - Hf\|^2}{2\sigma^2}\right) \quad (7)$$

where σ^2 is the Gaussian noise variance, $\|\cdot\|$ is the Euclidean norm.

III. PROPOSED ALGORITHM

A. A PRIOR DISTRIBUTION OF THE IMAGE

A Bayesian estimation technique needs to be provided a meaningful prior probability, which becomes a shortcoming. Several different approaches of the image a prior probabilities were proposed in [5], [6], [13]. Some approaches are suitable for a specific class of images and others are more general. The classical form selects the Laplacian operator as the inverse of the covariance matrix of f, but it does not fit for the prior model, since the L_2 norm of the image gradient penalizes too much the gradients around edges and an oversmoothing effect is observed [13].

Because a prior image distribution consists of a convex function of measures, here we use the Huber-Markov random field (HMRF) to model the prior distribution $P(f)$. To model the image, a Markov random field (MRF) is assumed with the Gibbs density function [6]

$$P(f) = \frac{1}{Z} \exp\left\{-\frac{1}{\zeta}\sum_{c\in C} \rho(d_c^T f)\right\} \quad (8)$$

where Z is a normalization constant, ζ is the "temperature" of the density, points c is called cliques, C denotes the set of all cliques throughout the image, d_c is a coefficient vector for clique c, the superscript notation $(\cdot)^T$ in Eq. (8) is the transpose operator, and $\rho(\cdot)$ is a function satisfying the following properties: convexity, symmetry, and reduced growth at regions of discontinuities, i.e., for a large $|v|$, $\rho(v) \ll v^2$ [6].

Among functions which satisfy these properties, the Huber function is considered, and it is defined as

$$\rho(v) = \begin{cases} v^2, & |v| \leqslant \xi \\ \xi^2 + 2\xi(|v| - \xi) & |v| > \xi \end{cases} \quad (9)$$

where ξ is the Huber threshold which controls the transition between L_1 and L_2 norms. The Huber function is convex and nonquadratic when $\xi < \infty$ [7].

B. A PRIOR DISTRIBUTION OF THE BLUR KERNEL

The marginalized probability $P(h)$ can be expressed in a closed form only for simple priors, such as variational Bayes [9] or the Laplacian distribution [8], [11], that can be used. For the blur kernel prior distribution, we use Laplacian distribution on the positive PSF values to force sparsity and zero on the negative values. The kernels h_m can be of different sizes, and the largest size is $L \times L$ ($L \ll N_1, N_2$). In oder to guarantee positivity and sparsity, we present to use an effective blur kernel regularizer, so a prior distribution $P(h)$ can be defined as

$$P(h) \propto \exp\left\{\frac{1}{\alpha} h^T Q_\Delta h + \Phi(h)\right\} \quad (10)$$

where α is the weight that controls the effect of the multi-frame constraint Q_Δ, Q which is a matrix with Δ denoting a convolution with the discrete Laplacian kernel l (in 1-D case, $l = [1, -2, 1]$), the Q_Δ is defined as [11]

$$Q_\Delta = [\Delta G_2, -\Delta G_1]^T [\Delta G_2, -\Delta G_1] \quad (11)$$

where matrix Q_Δ depends only on the input images g_m, and the construction is trivial. The function $\Phi(\cdot)$ forces sparsity by computing the L_1 norm of positive PSFs and ensures positivity by absolutely penalizing negative values. It is given as

$$\Phi(h(x)) = \sum_{m=1}^{M}\sum_{x=1}^{L} \varphi(h_m(x)) \quad (12)$$

where

$$\varphi(v) = \begin{cases} v, & v \geq 0 \\ +\infty & v < 0 \end{cases} \quad (13)$$

C. ALTERNATING MINIMIZATION FOR MAP ESTIMATION

Combining with the prior distributions presented in Eq. (7), Eq. (8), and Eq. (10), from Eq. (6), we can obtain the negative log-likelihood which is shown in Eq. (14)

$$\begin{aligned} J(\hat{f}, \left\{\hat{h}_m\right\}) &= \arg\min_{\{f,\{h_m\}\}} \{-\log P(g|f, \{h_m\}) - \log P(f) \\ &\quad - \log P(\{h_m\})\} \\ &= \sum_x \left\{\frac{N_1N_2}{2} \ln\sigma^2 + \frac{\|g(x) - Hf(x)\|^2}{2\sigma^2}\right\} \end{aligned}$$

$$+\sum_x\left\{\frac{1}{\zeta}\sum_{c\in C}\rho(d_c^T f(x))\right\}$$
$$+\sum_x\left\{\frac{1}{\alpha}h^T(x)Q_\Delta h(x)+\Phi(h(x))\right\} \quad (14)$$

Minimizing Eq. (6) is equal to minimizing $J(\hat{f},\{\hat{h_m}\})$. The standard method to solve Eq. (14) is called alternating minimization algorithm (AM) [11] and will be adopted here as well. The AM algorithm is summarized as follows,

"f-step":

$$\min_f\{-\log P(g|f,\{h_m\})-\log P(f)\} \quad (15)$$

"h-step":

$$\min_{\{h_m\}}\{-\log P(g|f,\{h_m\})-\log P(\{h_m\})\} \quad (16)$$

and alternate between them.

The AM algorithm which solves the multiframe AO images restoration problem, consists of two subproblems: minimization with respect to the image regularization term (f-step) and the minimization with respect to the blur regularization term (h-step). Accoring to the AM algorithm, the numerical iterative process is then obtained,

$$\hat{h}_t^{k+1}(x)=\hat{h}^k(x)\left\{\hat{f}^k(x)\otimes\left[\frac{\hat{f}^k(x)\otimes\hat{h}^k(x)-g(x)}{\sigma^2}\right]\right\}\times\frac{1}{1+\sum_{x\in\Omega}\frac{1}{\alpha}Q_\Delta\hat{h}^k(x)}, \quad (17)$$

$$\hat{h}^{k+1}(x)=\frac{\hat{h}_t^{k+1}(x)}{\sum_{x\in\Omega}\hat{h}_t^{k+1}(x)} \quad (18)$$

and

$$\hat{f}^{k+1}(x)=\hat{f}^k(x)\left\{\hat{h}^{k+1}(x)\otimes\left[\frac{\hat{f}^k(x)\otimes\hat{h}^{k+1}(x)-g(x)}{\sigma^2}\right]\right\}\times\frac{1}{1+\frac{1}{\zeta}\sum_{c\in C}d_c\rho'(d_c^T\hat{f}^k(x))} \quad (19)$$

where the superscript indexes the number of iteration, and $\rho'(v)$ denotes the first order derivative of the function $\rho(v)$,

$$\rho'(v)=\begin{cases}2v, & |v|\leqslant\xi\\ 2\xi\dfrac{v}{|v|} & |v|>\xi\end{cases} \quad (20)$$

where ξ is a threshold for the Huber function.

D. IMPLEMENTATION

We have analyzed the main steps (f-step and h-step) of the proposed algorithm. Now we proceed with the description of the main loop of the algorithm. Using Eqs. (17)-(18), and Eq. (19), the estimation for the object image $\hat{f}$ and the PSF $\hat{h}$ are obtained by iterations. The pseudo-code for our algorithm is summarized in Algorithm 1.

Algorithm 1 Steps for Our Proposed Algorithm

Step 1: Initialize operation. The $M(M\geq 2)$ frames of input images $\{g_1,g_2,\ldots,g_M\}$ are obtained with frame selection technique [17], then the initial object image is $\hat{f}^0=(g_1+g_2+\cdots+g_M)/M$;

Step 2: Obain the initial estimation of the PSF, $\hat{h}_t^0(x)$, is to delta functions, calculate Q_Δ, and choose the values of parameters d_c, α, ζ, and ξ;

Step 3: Iterate through $j = 1, 2, \ldots, MaxIteration$ ($MaxIteration = 200$ or 300):

1) The inner loop count variable of PSF $h\_count = 0$;
2) (h-step) The iteration process of PSF estimation, $k = 0, 1, \ldots, Max\_count$;
   a) Complete the PSF estimation $\hat{h}^k$ using optimized Eqs. (17)-(18);
   b) Increase h_count; Increase k;
   c) Check the value of the loop variable k: if $k < Max\_count$, continue; otherwise, go to *Step* 3 (3).
3) The inner loop counter variable of object estimation: $f\_count = 0$;
4) (f-step) The iteration process of object estimation, $q = 0, 1, \ldots, Max\_count$;
   a) The conjugate gradient method was used to optimize Eq. (19) and to obtain object image estimation $\hat{f}^q$;
   b) Increase f_count; Increase q;
   c) Check loop variable q: if $q < Max\_count$, continue; otherwise, go to *Step* 3 (5);
5) Check whether the extrinsic loop is over, if $j > MaxIteration$, then go to **Step 4**;
6) Increase j, return to *Step* 3 (1).

Step 4: If $j > MaxIteration$, then output object estimate image $\hat{f}$ and PSF estimation $\hat{h}$, and end the algorithm; otherwise go to **Step 3**.

#name	switch	type	values
algorithm	"--"	categorical	(acs)
alpha	"--alpha "	real	(10, 100000)
zeta	"--zeta "	real	(1.0,10000)
sigma^{2}	"-- sigma^{2}"	real	(0,5.0)
xi	"--xi "	real	(0,2.0)

FIGURE 2. The parameter file(parameter1.txt). The first column is the parameter name; the second column is a label;the third column is the parameter type;and the fourth column gives the range or domain.

In our method, parameter settings is based on the irace package [21]. First, we define a parameter file(parameter1.txt, Fig. 2). Then, we create a scenario file(set $maxExperiments =$ 1000 runs of ACOTSP [21], which is an applications of irace.) We create a basic target-runner-run script that runs the ACOTSP software and prints the objective value of the best solution found.

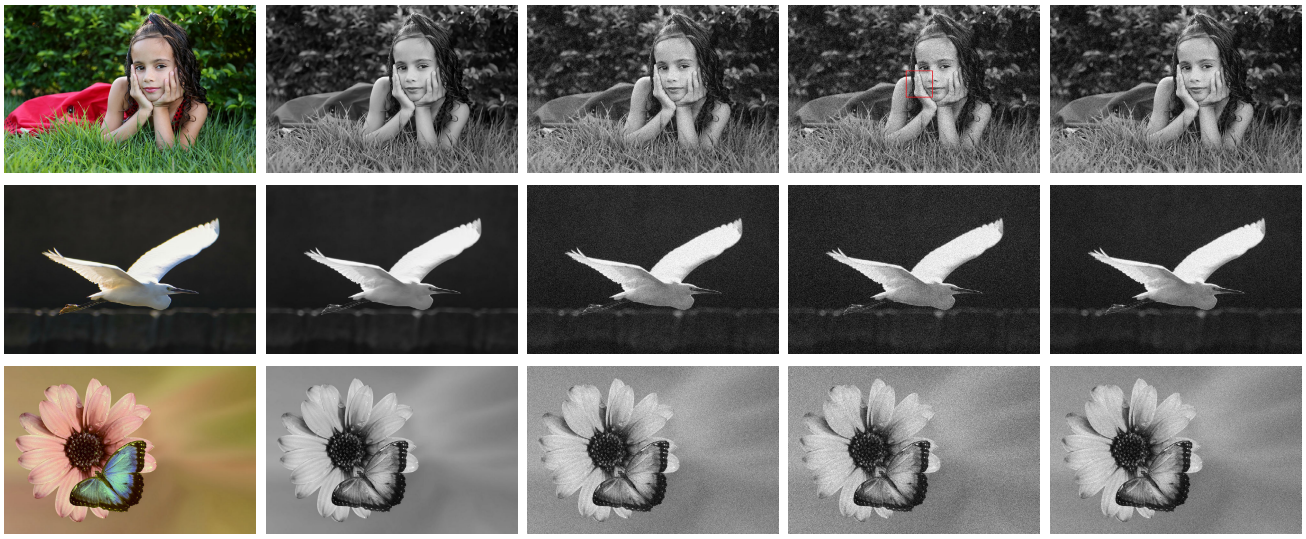

FIGURE 3. Original 640 × 960 images and simulated degraded images with the PSF size set to 7 × 7. (a) original images used for simulations; (b) the gray images of (a); (c)-(e): degraded images for three different noise levels: 50 dB, 35 dB, and 25 dB under ideal conditions.

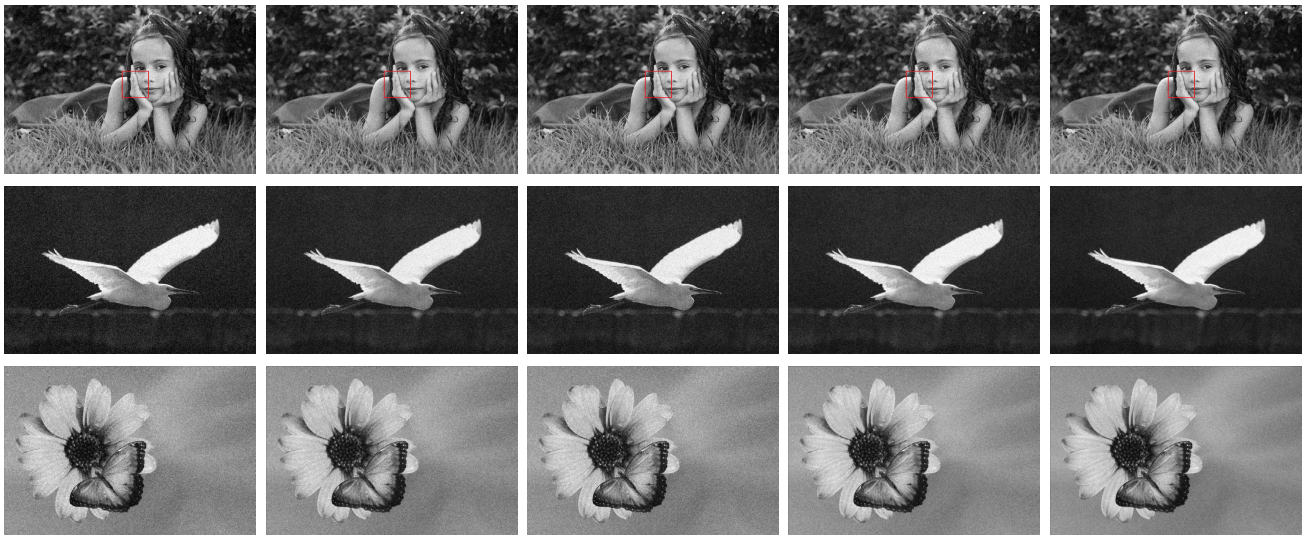

FIGURE 4. Restoration result comparisons using five methods (with 150 iterations). (a) the RL-IBD method; (b) the ML-EM method; (c) the CPF-adaptive method; (d) the RMF-MLE method; (e) our method with $\xi = 1$ and $\sigma^2 = 1.7$.

At the end of a run, irace prints the best configurations found as command-line parameters. We have noticed that, in general, the parameters can be fixed relative to one of variables, e.g., α, which depends on the noise level. In this case, ζ, with respect to the weight α of the fidelity term can be determined. The rule of thumb is to set α to a ratio of signal and noise variances. That is, with SNR = 50 dB, α can be set to 10^5 or with SNR = 30 dB, α can be set to 10^3. Then, we found that choosing $\zeta = 10^{-1}\alpha$ usually results in better convergence. The up-sample ratio was $L_1 = L_2 = 5$. In our case, we used a Gaussian blur with variance $\sigma^2 = 1.7$. The variance of noise is estimated at a ''smooth'' area of a low-resolution. The threshold for the Huber function is set at $\xi = 1$ for our method.

IV. EXPERIMENTAL RESULTS

In this section, we demonstrate the performance of our algorithm on simulated images and real adaptive optics images. First, the simulated data for different SNR are used to compare results of the RL-IBD method [23], the ML-EM method [24], the CPF-adaptive method [25], the RMF-MLE method [26], and our method. Second, the performance of our method is evaluated on adaptive optics images taken by a 1.2 m AO telescope from Yunnan

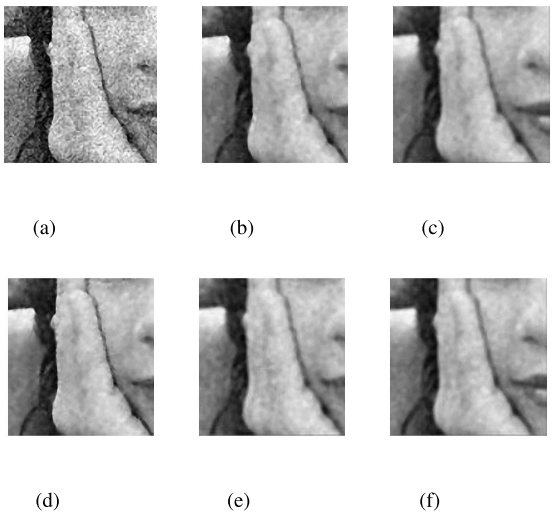

FIGURE 5. Close-ups of degraded/restoration image regions extracted from Girl images in Fig. 3(c) and Fig. 4. (a) is from Fig. 3(c); (b)-(f) are from restored Girl image regions extracted from Fig. 4(a)-(e), respectively.

Observatory, China. The main parameters for this telescope are: the atmospheric coherence length $r_0 = 13$ cm, telescope diameter $D = 1.08$ m, the pixel size of CCD is 7.4 μm, focal length $l = 22.42$ m, the wavelength in center $\lambda = 700$ nm. Moreover, all algorithms were implemented in Matlab and executed on a standard PC with a 2.7 GHz Intel i7-7500U CPU and 8.0 GB RAM, running on a 64 bit Windows 10 operating system.

For the evaluation on the performance for the simulated data and real AO data, we use percentage mean squared errors (E_{PMSE}) [13], peak signal to noise ratio(E_{PSNR}), and Laplacian sum (E_{LS}) [20]. The E_{PMSE} is used for the estimated PSF $\hat{h}$ and for the estimated restored image $\hat{f}$, respectively, defined as follows

$$E_{\text{PMSE}}(f(x,y)) = 100 \times \frac{\|\hat{f}(x,y) - f(x,y)\|}{\|f(x,y)\|},$$
$$E_{\text{PMSE}}(h(x,y)) = 100 \times \frac{\|\hat{h}(x,y) - h(x,y)\|}{\|h(x,y)\|} \quad (21)$$

where (x, y) is a pixel location. Both $\hat{h}(x, y)$ and $\hat{f}(x, y)$ are the outputs of our method.

The E_{PMSE} is a measure of the quality of an estimator of the overall deviations between the original image and the object image, and it is always non-negative, and a value close to zero is better. A lower E_{PMSE} value indicates that the deviation is small and a better restored result is obtained.

The E_{PSNR} is the ratio of the maximum signal to the noise level, and is defined as

$$E_{\text{PSNR}} = 10\log\left(\frac{\max_{x,y}(f(x,y) - \hat{f}(x,y))^2}{\frac{1}{MN}\sum_{x=1}^{M}\sum_{y=1}^{N}(f(x,y))^2}\right) \quad (22)$$

The E_{LS} is for very pixel in a 3×3 neighborhood after applying the Laplacian operator, and getting the differential value of eight neighborhood, and then summing in the range of image. It is defined as

$$E_{\text{LS}} = \frac{\sum_{x=2}^{M-1}\sum_{y=2}^{N-1}|A(x,y)|}{(M-2)(N-2)} \quad (23)$$

where

$$\begin{aligned} A(x,y) = {} & 8g(x,y) - g(x,y-1) - g(x-1,y) - g(x,y+1) \\ & -g(x-1,y-1) - g(x-1,y+1) \\ & -g(x+1,y-1) - g(x+1,y+1) \end{aligned} \quad (24)$$

where M and N represent the total number of pixels along the x-axis and y-axis of the image, respectively. $g(x, y)$ denotes the degraded image or the restored image. A higher E_{LS} value indicates that a better restored result is obtained.

A. SIMULATED DATA EXPERIMENT

In the simulated data experiment, we run our restoration method on three standard datasets [22] "Girl" (640 × 960 pixels), "Animal" (640 × 960 pixels), and "Flower" (640 × 960 pixels) to test the performance of our proposed method. The parameters are set the same as the 1.2 m AO telescope on Yunnan Observatory, China. The set of experiments compares the proposed method with the RL-IBD method [23], the ML-EM method [24], the CPF-adaptive method [25], and the RMF-MLE method [26].

The setup for the simulated data experiment was the following. Fig. 3 is the test data set, including the original images and degraded images. We select the "Girl", "Animal", and "Flower" images from the datasets [22] are shown in Fig. 3(a), and the corresponding gray images are shown in Fig. 3(b). The images are convolved with 7×7 blurs and noises are added at three different levels with SNR = 50 dB, 35 dB, and 25 dB with real AO imaging conditions including atmospheric turbulence as shown in Fig. 3(c)-(e). The comparison results based on the five methods are shown in Fig. 4. In our method, the parameters $\xi = 1$ and $\sigma^2 = 1.7$ were selected experimentally for visually acceptable results by using the irace package [21]. The results shown in Fig. 4(a) contain significant noise, indicating that the algorithm has poor noise suppression ability. Images Fig. 4(b) exhibit an obvious block effect, which worsens the visual effect of the image. Images Fig. 4(c) has better brightness, but the image appears a smooth transition. Images Fig. 4(d) and (e) have the best overall consistency and similar restoration results, although (e) superior to (d) in terms of texture details and anti-noising. In Fig. 5, we select certain parts from the "Girl" blurred image in Fig. 3(c), and the corresponding areas from the four restoration images, which are shown in Fig. 5(b)-(f). From Fig. 5(f), we can see that the contours of face and hand become clearer, which demonstrates that the proposed method is effective.

The reference evaluation results of the restored images from high-degradation images(Fig. 3) are presented in Table 1. Table 1 gives the results of our method and

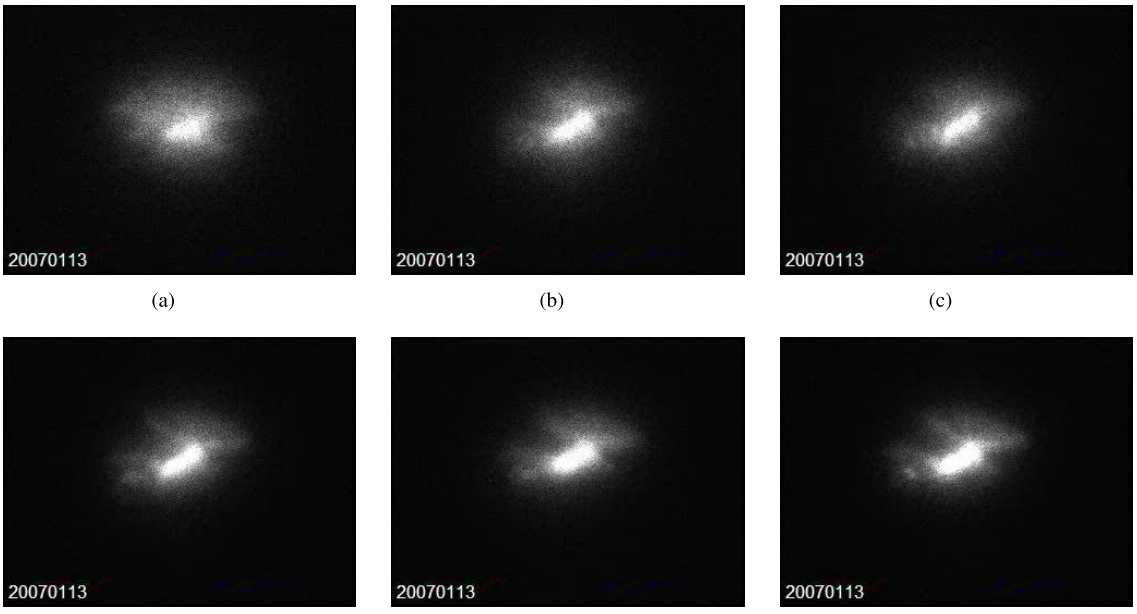

FIGURE 6. Six frames of the observed flying object AO images and their variances. (a) Frame 1 with variance $S_1^2 = 427.91$; (b) Frame 2 with variance $S_2^2 = 423.62$; (c) Frame 3 with variance $S_3^2 = 431.79$; (d) Frame 4 with variance $S_4^2 = 418.65$; (e) Frame 5 with variance $S_5^2 = 435.53$; (f) Frame 6 with variance $S_6^2 = 427.91$.

TABLE 1. Performance of the five methods on simulated data in Fig. 4.

Image names	RL-IBD		ML-EM		CPF-adaptive		RMF-MLE		Our method	
	E_{PMSE}	E_{PSNR}	E_{PMSE}	E_{PSNR}	E_{PMSE}	E_{PSNR}	E_{PMSE}	E_{PSNR}	E_{PMSE}	E_{PSNR}
Girl	4.33	21.07	4.25	21.96	4.03	19.84	4.17	22.36	**3.96**	**24.83**
Animal	6.28	21.62	6.17	21.79	6.07	20.94	5.98	25.59	**5.59**	**25.94**
Flower	5.37	22.13	6.04	22.59	5.28	23.16	4.73	24.77	**4.27**	**25.12**

those of the RL-IBD method [23], the ML-EM method [24], the CPF-adaptive method [25], the RMF-MLE method [26], and the iteration number for the five methods is 150. The results indicate that our proposed method via regularization priors achieves the best performance, especially in providing better object estimation and preserving boundaries.

B. FLYING-OBJECT AO IMAGE EXPERIMENT

The last test which we have conducted was on the real adaptive optics images obtained in the observation of a flying object. The restoration experiment on the flying object images is carried out using our proposed algorithm. Since the atmospheric conditions may change very quickly, the observed AO image sequence usually contains different quality from sharp to heavy blurred ones. The flying object images for the experiment were taken by a 1.2 m AO telescope from the Chinese Academy of Sciences in Yunnan Observatory on January 13, 2007. The AO system parameters are the same as that at the beginning of Section IV. The initial estimated PSF model for the anisoplanatic effect for the flying-object image is as follows: the grid of space-variant PSF is 3×3; the isoplanatic angle θ is $2''$; the field-of-view is $10''$; the full field-of-view for the system is $20''$; and the Zernike model is with the first 35 orders. In the experiment, we chose $\alpha = 10^2$, $\zeta = 10^{-1}\alpha$, $\sigma^2 = 1.83$, the threshold for the Huber function is set at $\xi = 1.2$ for visually acceptable results based on the irace package [21]. Then, we compared the performance of the proposed restoration strategy using our algorithm with those of blind deconvolution strategies, including the RL-IBD method [23], the ML-EM method [24], the CPF-adaptive method [25], and the RMF-MLE method [26]. The frame selection method which is introduced in [26] is applied, and 50 frames are selected from 200 frames of degraded AO images on a flying object as blind convolution images. The degraded AO images on the flying object are given in Fig. 6 (only 6 frames of the AO images are shown). Moreover, we have calculated the variance for each observed AO image in Fig. 6, and their values are close to each other between 418 and 436.

In the restoration process, Eqs. (18) and (19) are iterated for 200 times. We can obtain the restoration results based on our proposed method which are shown in Fig. 7 with comparison results based on four other methods. Fig. 7(a) is the restored image by the RL-IBD method with $E_{\text{PMSE}} = 13.03$ and $E_{\text{LS}} = 5.2466$; Fig. 7(b) is the restored image by

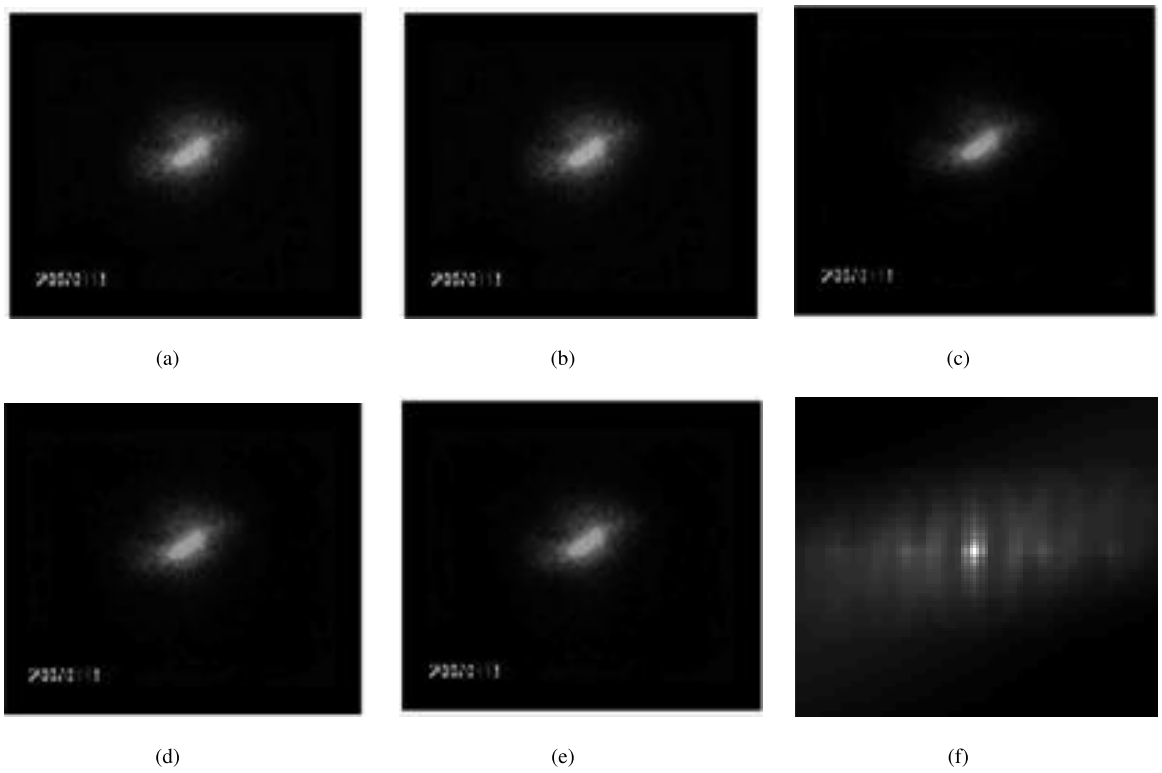

FIGURE 7. The comparison of restored results on observed flying object AO images using five methods. (a) Result from the RL-IBD method; (b) Result from the ML-EM method; (c) Result from the CPF-adaptive method; (d) Result from the RMF-MLE method; (e) Result from our method; (f) Estimated PSF by our method.

the ML-EM method with $E_{\text{PMSE}} = 12.51$ and $E_{\text{LS}} = 5.0203$; Fig. 7(c) is the restored image by the CPF-adaptive method with $E_{\text{PMSE}} = 12.08$ and $E_{\text{LS}} = 5.3786$; Fig. 7(d) is the restored image by the RMF-MLE method with $E_{\text{PMSE}} = 11.79$ and $E_{\text{LS}} = 5.3059$; Fig. 7(e) is the restored image using our method with $E_{\text{PMSE}} = 10.24$ and $E_{\text{LS}} = 6.0633$ for 200 iterations; and Fig. 7(f) shows the resulting PSF by our method. Note that the PSF tends to become discrete. We observe that the PSF enhances the image, providing brighter active regions and darker background regions with low intensities than in the original image. Fig. 8 is the plot on the energy spectra for the five restoration methods. Fig. 8(a) is the energy on the restored image in Fig. 7(a) based on the RL-IBD method; Fig. 8(b) is the energy on the restored image in Fig. 7(b) based on the ML-EM method; Fig. 8(c) is the energy on the restored image in Fig. 7(c) based on the CPF-adaptive method; Fig. 8(d) is the energy on the restored image in Fig. 7(d) based on the RMF-MLE method; and Fig. 8(e) is the energy on the restored image in Fig. 7(e) based on our method. With the comparison, it shows that the proposed method is better than the other four methods.

Table 2 are the E_{PMSE}, E_{LS}, and computation time comparison on the restored flying object AO images (iteration number is 300). Comparing with the RL-IBD, ML-EM, CPF-adaptive, and RMF-MLE methods, we can see that the E_{PMSE} measures from our method are decreased by 19.9%, 16.7%, 10.6%, and 8.6%, respectively. It can be seen that our method has achieved the smallest E_{PMSE} value among the five methods, and the E_{LS} value from our method is higher than those from the others. From the computation time of the experimental results, the time of our method is slightly higher

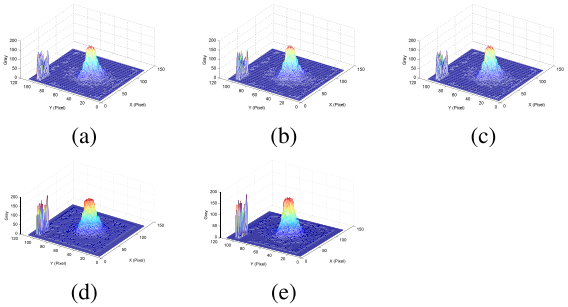

FIGURE 8. Energy spectra comparison for the restored AO images from the five methods. (a) Energy of the restored image using the RL-IBD method on Fig. 7(a); (b) Energy of the restored image using the ML-EM method on Fig. 7(b); (c) Energy of the restored image using the CPF-adaptive method on Fig. 7(c); (d) Energy of the restored image using the RMF-MLE method on Fig. 7(d); (e) Energy of the restored image using our method on Fig. 7(e).

TABLE 2. The E_{PMSE}, E_{LS}, and computation time calculated for the flying object images (iteration number is 300).

Methods	E_{PMSE}	E_{LS}	Computation time (s)
RL-IBD	11.23	6.3725	15.015
ML-EM	10.87	6.5027	14.673
CPF-adaptive	10.06	6.981	**13.802**
RMF-MLE	9.84	7.106	14.201
Our method	**8.99**	**7.502**	15.072

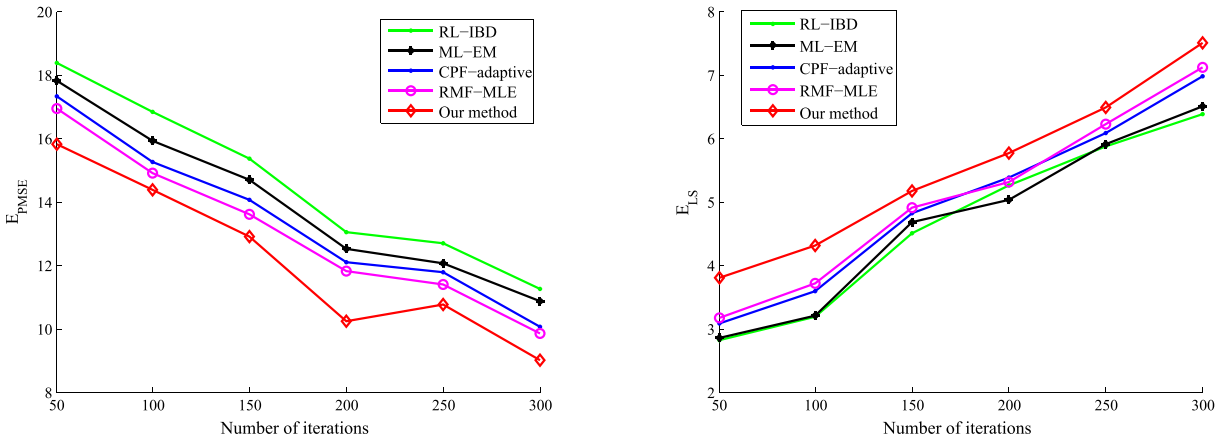

(a) (b)

FIGURE 9. The restoration comparisons on E_{PMSE} and E_{LS} measures versus the iteration number for the five methods. (a) E_{PMSE} versus the iteration number of the five methods. (b) E_{LS} versus the iteration number of the five methods.

than that of the other methods. In order to reduce the computation time, some functions such as the proximity operators may be computed in parallel because many of the convex functions on which they are defined are separable [27]. If our algorithm is implemented in C++ instead of MATLAB, the time spent can also be reduced.

Moreover, Fig. 9 shows that the E_{PMSE} and E_{LS} measures of our method and those of other restoration methods such as RL-IBD, ML-EM, CPF-adaptive, and RMF-MLE. The E_{PMSE} measure versus the iteration number for the five restoration methods on the flying object AO images are plotted in Fig. 9(a). Fig. 9(b) is the E_{LS} results for the five restoration methods. One can see that the proposed method provides accurate results and shows robustness with respect to noise. Our method ranks on the top of the list, and the results demonstrate the superiority of our method.

C. COMPUTATIONAL COMPLEXITY ANALYSIS

Let N denote the number of pixels in the output image f, and Let $\hat{L}$ denote the pixels in PSF support. The calculation of Q_Δ can use the fast Fourier transform(FFT), thus the overall complexity is $O(K\hat{L}N\log N)$. In general, the most time-consuming is the f-step, which requires an inversion of the huge $N \times N$ matrix. To avoid any ringing artifacts close to image boundaries, we should perform valid convolution, for example, the output image is smaller and covers a region where both the convolution kernel and input image are fully defined. The TV regularizer [28] can help to reduce such artifacts. Therefore, the f-step performed with an overall $O(N\log N)$ cost.

The h-step is performed in the image domain, since we need constrain kernel support $\hat{L}$. Otherwise, Q_Δ becomes a very uninformative regularizer. On the h-step method, we have to invert matrix and thus much smaller than the matrix in the f-step. Typically, for two input images ($K = 2$), and the size of blurs is not more than 30×30 pixels($L = 900$), the matrix size is 1800×1800 which is relatively small. One can apply a conjugate gradient to solve the iterative problem. This can be computed in $O((K\hat{L})^3)$ time. Again, the update steps for k and h_count require $O(K\hat{L})$ operations.

V. DISCUSSIONS AND CONCLUSIONS

This paper presents a novel method for solving adaptive optics image restoration. There are two main contributions in this paper. The first contribution was that we defined prior distributions for image and blur regularization terms, which help for the solving of ill-posed problems when estimating the true image from observations. The image regularization is formulated using the Huber-Markov random field. For the blur kernel prior distribution, we use Laplacian distribution on the positive PSF values to force sparsity and zero on the negative values. The second contribution is that we solve the optimization problem in an iterative way by alternating between minimization with respect to the image (f-step) and with respect to the PSFs (h-step), which can solve each step efficiently and reduce the computational complexity as well. Experimental results illustrated both quantitatively and qualitatively that our proposed method outperforms the state-of-the-art methods on both synthetic degraded images and real AO images, but at a slightly more computational cost. To overcome this computational speed issue, our future research can focus on parallel computing.

ACKNOWLEDGMENT

The authors would like to thank the authors for the Pixabay image databases. They would also like to thank the anonymous reviewers for their helpful and constructive comments.

REFERENCES

[1] M. Van Noort, L. R. Van Der Voort, and M. G. Löfdahl, "Solar image restoration by use of multi-frame blind de-convolution with multiple objects and phase diversity," *Solar Phys.*, vol. 228, nos. 1–2, pp. 191–215, May 2005.

[2] L. M. Mugnier, T. Fusco, and J.-M. Conan, "MISTRAL: A myopic edge-preserving image restoration method, with application to astronomical adaptive-optics-corrected long-exposure images," *J. Opt. Soc. Amer. A, Opt. Image Sci.*, vol. 21, no. 10, pp. 1841–1854, Oct. 2004.

[3] T. R. Rimmele, "Solar adaptive optics," *Astronomical Telescopes Instrum.*, vol. 4007, pp. 218–231, Jul. 2000.

[4] L. Xu and J. Jia, "Two–phase kernel estimation for robust motion deblurring," in *Proc. Eur. Conf. Comput. Vis.*, 2010, pp. 157–170.

[5] J. Kotera, F. Šroubek, and P. Milanfar, "Blind deconvolution using alternating maximum a posteriori estimation with heavy-tailed priors," in *Proc. Int. Conf. Comput. Anal. Images Patterns*, 2013, pp. 59–66.

[6] R. Schultz and R. Stevenson, "A Bayesian approach to image expansion for improved definition," *IEEE Trans. Image Process.*, vol. 3, no. 3, pp. 233–242, May 1994.

[7] R. Pan and S. J. Reeves, "Efficient Huber–Markov edge-preserving image restoration," *J. Opt. Soc. Amer. A, Opt. Image Sci.*, vol. 15, no. 12, pp. 3728–3735, 2006.

[8] N. P. Galatsanos, V. Z. Mesarovic, R. Molina, and A. K. Katsaggelos, "Hierarchical Bayesian image restoration from partially known blurs," *IEEE Trans. Image Process.*, vol. 9, no. 10, pp. 1784–1797, Oct. 2000.

[9] J. Miskin and D. J. C. Mackay, "Ensemble learning for blind image separation and deconvolution," in *Advances in Independent Component Analysis* (Perspectives in Neural Computing). London, U.K.: Springer, 2000, pp. 123–141.

[10] M. Charbit, *Digital Signal and Image Processing Using MATLAB*, vol. 666. Hoboken, NJ, USA: Wiley, 2010, pp. 9–23.

[11] F. Sroubek and P. Milanfar, "Robust multichannel blind deconvolution via fast alternating minimization," *IEEE Trans. Image Process.*, vol. 21, no. 4, pp. 1687–1700, Apr. 2012.

[12] S. Babacan, R. Molina, and A. Katsaggelos, "Variational Bayesian blind deconvolution using a total variation prior," *IEEE Trans. Image Process.*, vol. 18, no. 1, pp. 12–26, Jan. 2009.

[13] F. Sroubek and J. Flusser, "Multichannel blind iterative image restoration," *IEEE Trans. Image Process.*, vol. 12, no. 9, pp. 1094–1106, Sep. 2003.

[14] A. Levin, Y. Weiss, F. Durand, and W. T. Freeman, "Understanding and evaluating blind deconvolution algorithms," in *Proc. IEEE Conf. Comput. Vis. Pattern Recognit.*, Jun. 2009, pp. 1964–1971.

[15] N. Joshi, R. Szeliski, and D. J. Kriegman, "PSF estimation using sharp edge prediction," in *Proc. IEEE Conf. Comput. Vis. Pattern Recognit.*, Jun. 2008, pp. 1–8.

[16] G. R. Ayers and J. C. Dainty, "Iterative blind deconvolution method and its applications," *Opt. Lett.*, vol. 13, no. 7, p. 547, Jul. 1988.

[17] T. Yu, R. Chang-hui, and W. Kai, "Adaptive optics image restoration based on frame selection and multi-frame blind deconvolution," *Chin. Astron. Astrophys.*, vol. 33, no. 2, pp. 223–230, Apr. 2009.

[18] L. Zhang, D. Li, W. Su, J. Yang, and Y. Jiang, "Research on adaptive optics image restoration algorithm by improved expectation maximization method," *Abstract Appl. Anal.*, vol. 2014, Jul. 2014, Art. no. 781607.

[19] K. H. Yap, "Adaptive image restoration based on hierarchical neural networks," *Opt. Eng.*, vol. 39, no. 7, pp. 1877–1890, Jul. 2000.

[20] J. Tang, *Regularization Method for Image Restoration*. Wuhan, China: Huazhong Univ. of Science and Technology, 2006, pp. 101–113.

[21] M. López-Ibáñez, J. Dubois-Lacoste, L. P. Cáceres, M. Birattari, and T. Stützle, "The irace package: Iterated racing for automatic algorithm configuration," *Oper. Res. Perspect.*, vol. 3, pp. 43–58, Jan. 2016.

[22] Pixabay. (2018). *The Pixabay Image Database: Free High Quality Images*. Accessed: Nov. 12, 2018. [Online]. Available: https://pixabay.com/en/

[23] F. Tsumuraya, N. Miura, and N. Baba, "Iterative blind deconvolution method using Lucy's algorithm," *Astron. Astrophys.*, vol. 282, no. 2, pp. 699–708, 1994.

[24] L. A. Shepp and Y. Vardi, "Maximum likelihood reconstruction for emission tomography," *J. Opt. Soc. Amer. A, Opt. Image Sci.*, vol. 1, no. 2, pp. 113–122, 1982.

[25] D. Zhu, M. Razaz, and M. Fisher, "An adaptive algorithm for image restoration using combined penalty functions," *Pattern Recognit. Lett.*, vol. 27, no. 12, pp. 1336–1341, Sep. 2006.

[26] D. Li, C. Sun, J. Yang, H. Liu, J. Peng, and L. Zhang, "Robust multi–frame adaptive optics image restoration algorithm using maximum likelihood estimation with Poisson statistics," *Sensors*, vol. 17, no. 4, pp. 785–804, Apr. 2017.

[27] B. Chen, C. Cheng, S. Guo, G. Pu, and Z. Geng, "Unsymmetrical multi-limit iterative blind deconvolution algorithm for adaptive optics image restoration," *High Power Laser Particle Beams (China)*, vol. 2, pp. 313–318, Feb. 2011.

[28] A. Padcharoen, P. Kumam, and J. Martínez-Moreno, "Augmented lagrangian method for TV-l1-l2 based colour image restoration," *J. Comput. Appl. Math.*, vol. 354, pp. 507–519, Jul. 2019.

DONGMING LI received the M.E. degree from the Changchun University of Technology, Changchun, China, in 2006, where he is currently pursuing the Ph.D. degree with the College of Opto-Electronic Engineering. He was a Visiting Scholar with CSIRO, Australia, from 2016 to 2017. He then joined Jilin Agricultural University, Changchun, where he is also a Professor carrying out teaching and research on projects. His current research interests include computer vision, image analysis, and pattern recognition.

GUANGJIE QIU is currently pursuing the M.E. degree with the School of Information Technology, Jilin Agricultural University. His main research interests include image processing and medical image analysis.

LIJUAN ZHANG received the M.E. and Ph.D. degrees from the Changchun University of Science and Technology, Changchun, China, in 2004 and 2015, respectively. She was a Visiting Scholar with CSIRO, Australia, from 2016 to 2017. She is currently a Professor with the College of Computer Science and Engineering, Changchun University of Technology. Her research interests focus on image restoration, computer vision, and image analysis.